Particle acceleration signatures in a time-dependent one-zone SSC model of blazar flares

Paloma Thevenet[1], Andreas Zech[1], and Catherine Boisson[1]

[1]LUTh - Observatoire de Paris, Université PSL, Université Paris Cité, CNRS

Context

Rapid flux variability over a large range of wavelengths is a well-known signature of blazar emission, with variability time scales of the order of a few days and below frequently observed at high energies. Radiative models with varying degrees of complexity are generally successful in reproducing individual flare events or overall statistical behaviour, but the physical origin of blazar flares is still unclear. Our study focuses on the shape of light curves of **rapid flares** considered as individual events from compact emission regions. We have explored the parameter space of a **one-zone synchrotron self-Compton model** (Maraschi et al. 1992 (*1*), Bloom & Marscher 1996 (*2*)) for several physical scenarios leading to flares due to the injection from additional relativistic electrons, initial acceleration and re-acceleration of electrons due to **Fermi-I and Fermi-II mechanisms** (Matthews et al. 2020 (*3*)). The time-dependent EMBLEM code (Dmytriiev 2021 (*4*)) has been used to solve the kinetic equation describing the evolution of the electron distribution, simulate broad-band spectral distributions and multi-wavelength light curves, taking into account adiabatic expansion and the internal light-crossing effect. We have identified a few observable signatures in the shapes of the resulting light curves and in the relative amplitudes between different bands that are specific to these generic scenarios.

The Model

The evolution of the electron distribution $N_e(\gamma, t)$ within the blob is governed by the Fokker-Planck equation (Kardashev 1962 (*5*), Tramacere et al. 2011 (*6*)):

$$\frac{\partial N_e(\gamma,t)}{\partial t} = \underbrace{\frac{\partial}{\partial \gamma}[(b_c(\gamma,t)\gamma^2 + \frac{1}{t_{ad}}\gamma}_{\text{Cooling terms}} \underbrace{- a(t)\gamma - \frac{2}{\gamma}D_{F_{II}}(\gamma,t))N_e(\gamma,t)]}_{\text{Acceleration terms}} + \frac{\partial}{\partial \gamma}\left(D_{F_{II}}(\gamma,t)\frac{\partial N_e(\gamma,t)}{\partial \gamma}\right) - \underbrace{N_e(\gamma,t)\left(\frac{1}{t_{esc}} + \frac{3}{t_{ad}}\right)}_{\text{Cooling terms}} + \underbrace{\dot{Q}_{inj}(\gamma,t)}_{\text{Injection term}}$$

Cooling

- Synchrotron and Inverse Compton: $b_c(\gamma, t)$
- Adiabatic expansion: $t_{ad}(t) = \frac{R(t)}{\beta_{exp} c}$
- Escape: $t_{esc}^{(turb)} = \left(\frac{R_t}{c}\right)^2 \left(\frac{\delta B}{B}\right)^2 \frac{c}{\lambda_{max}} \left(\frac{r_L}{\lambda_{max}}\right)^{q-2}$

Acceleration

- Fermi I: $a = 1/t_{shock}$, $\dot{Q}(\gamma,t)$
- Fermi II: $D_{F_{II}}(\gamma, t) = \frac{p^2}{t_{F_{II}}}$

$$t_{F_{II}} = \frac{1}{\beta_A^2}\left(\frac{\delta B}{B}\right)^{-2} \frac{\lambda_{max}}{c}\left(\frac{r_L}{\lambda_{max}}\right)^{2-q}$$

We denote the electron momentum p, Larmor radius r_L, (variable) Alfvén speed β_A, turbulence level $\delta B/B$, longest wavelength in the Alfvén spectrum λ_{max} and slope of the turbulent spectrum q.
Blob parameters: comoving radius R, magnetic field B, Doppler factor δ, redshift z, Lorentz factor Γ, power-law electron distribution $\dot{Q}_{inj}$, expansion speed β_{exp}.

Evolving timescales: expansion timescale t_{ad}, turbulent escape timescale $t_{esc}^{(turb)}$, stochastic acceleration timescale $t_{F_{II}}$, synchrotron and synchrotron self-Compton (SSC) cooling rate b_c (no external photon fields).
Fixed timescales: escape timescale t_{esc} (for no turbulence), diffusive shock re-acceleration timescale t_{shock}.
The EMBLEM code solves the kinetic equation using a fully implicit difference scheme by Chang & Cooper 1970 (*7*), as described by Dmytriiev 2020 (*4*).
The **internal light crossing-effect** has been applied to the light curves similar to Tamacere 2020 (*8*).

Flare scenarios

- **Particle injection**: flaring through **additional particle injection** in the blob for a duration $t_{dur} = 3$ observer days ≈ 8 R/c, with constant injection spectrum $Q(\gamma)_{inj}$ and escape timescale $t_{esc} = 1$ R/c.
- **Injection and adiabatic expansion**: same flaring scenario as above including adiabatic expansion for an intrinsic opening angle $\alpha = \rho/\Gamma \approx 0.44°$ with $\rho = 0.26$ rad (Pushkarev et al. 2009 (*9*)).
- **Fermi I acceleration**: **diffusive shock acceleration** of cold plasma modelled through additional injection with energy-dependent cutoff $\dot{Q}(\gamma) = \dot{N}\left(\frac{\gamma}{\gamma_0}\right)^{\alpha} \exp\left(-\frac{\gamma}{\gamma_{cut}}\right)$ following Kirk et al. 1998 (*10*))
- **Fermi I re-acceleration**: **acceleration of a relativistic particle distribution on a shock** during $t_{dur} \approx 8$ R/c of timescale $t_{shock} = 1.3$ R/c modelled as systematic energy gain (term $a = 1/t_{shock}$).
- **Fermi II acceleration**: flaring through **stochastic acceleration** of a cold plasma for a duration $t_{dur} \approx 8$ R/c, with **time-dependent escape timescale** $t_{esc}^{(turb)}$. We consider only the 'hard-sphere' turbulence scenario for $q = 2$ and vary turbulence level $0 < \delta B/B \leq 1$ and maximum wavelength $0 < \lambda_{max} \leq R$.
- **Fermi II re-acceleration**: **stochastic acceleration of a relativistic particle distribution** using the same approach as above.

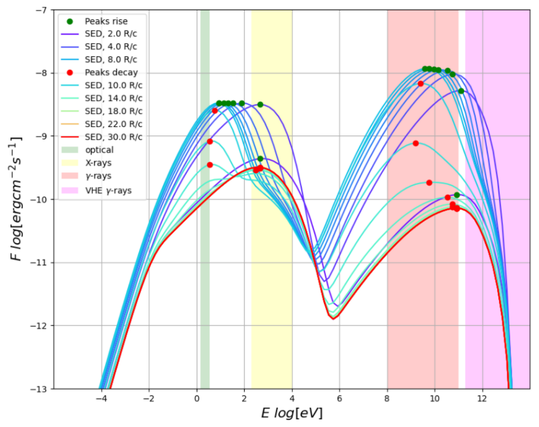

For each scenario we obtain the electron distribution evolution and the corresponding spectral energy distribution (SED). Integrating the SED in specific energy bands at each timestep, we recover the light curves (LC) for our domains of study: optical, X-rays, γ-rays and VHE γ-rays.

Figure 1: SED obtained for the case of Fermi II re-acceleration with $t_{FII} = 1.4$ R/c. The colored curves (purple - blue - green - red) represent the temporal evolution during the entire simulation. The first timestep is identical to the final one (red curve). The vertical bands correspond to the area integrated to compute the LCs in five energy bands: optical (green), X-rays (yellow), γ-rays (red) and VHE γ-rays (purple).

Example: light curves for initial acceleration scenarios

We present below the LCs in the case of Fermi I and Fermi II acceleration of cold particles in the optical and X-ray bands.

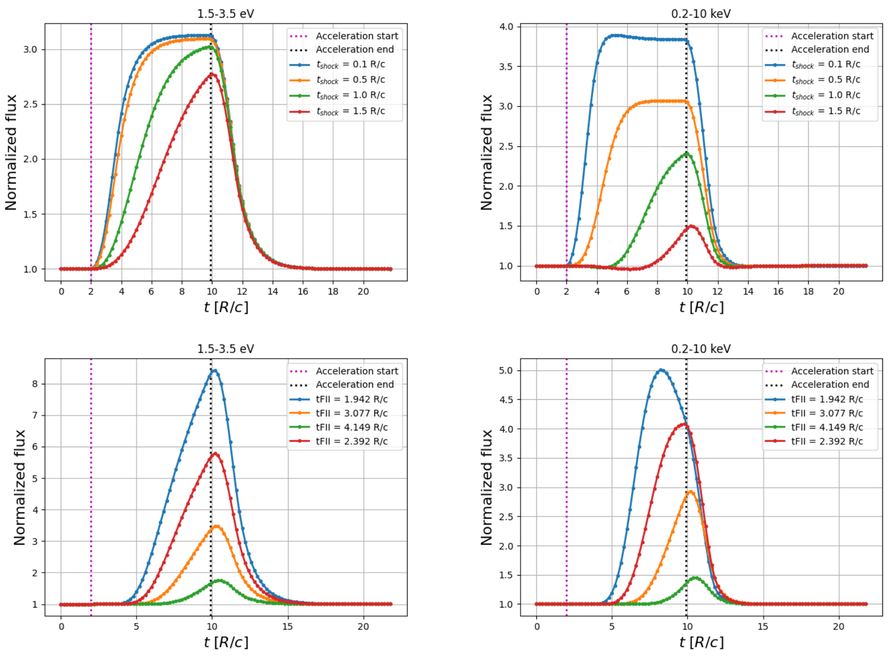

Figure 2: LCs comparison of the Fermi I (top) and Fermi II (bottom) acceleration scenarios in the optical (left) and X-ray (right) bands.

Comparison of the scenarios

We compare below the LCs for five flaring scenarios (excluding adiabatic expansion).
Parameters were chosen to obtain a similar variability amplitude in the optical band.

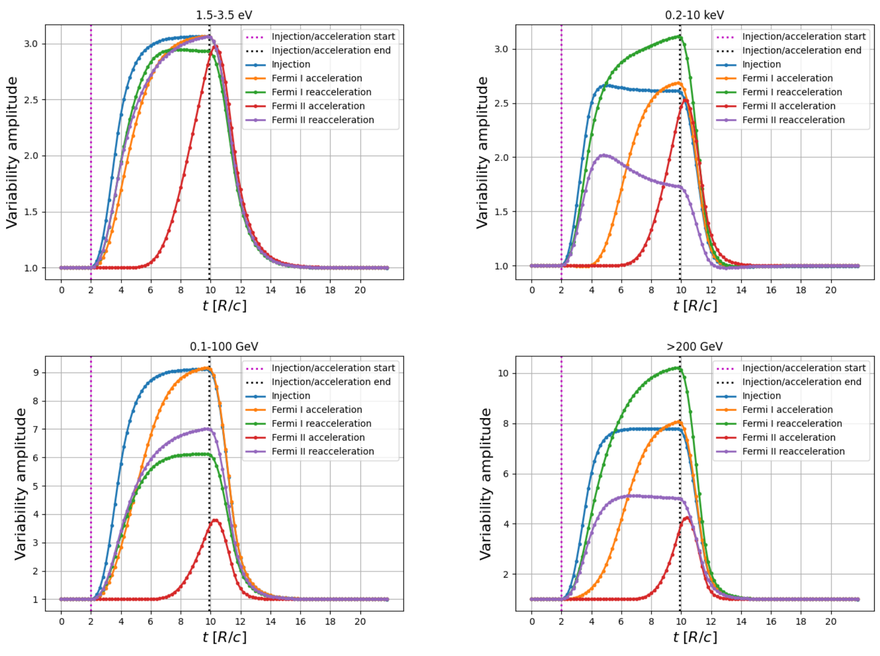

Figure 3: LCs comparison of five different flaring types. The flux evolution is given in the optical band (top left), X-ray band (top right), γ-ray band (bottom left) and VHE γ-ray band (bottom right).

Conclusions

Even within a single emission region, the different scenarios lead to a large variety of flare shapes and to large differences in the relative flux variability amplitudes (VA) between different bands. Exploring the parameter space, we identified LC signatures corresponding to different flaring scenarios.

- In the injection scenarios, the onset of the flare rise occurs at the same time in all bands. A plateau can be reached for a large range of VA, if the flare duration is sufficiently long. Adiabatic expansion (not shown here) leads to a visible flux decrease during the plateau phase.
- For the Fermi-I scenarios, the rise time is shorter for higher VAs. For shock acceleration of cold particles, the flare onset is delayed at higher energies, as expected.
- In the Fermi-II scenarios, the flare rise time is again shorter for higher VAs, while the flare onset occurs at the same time in different bands. Acceleration of cold particles never reaches a plateau for a large range of VAs. Efficient re-acceleration leads to a flare that is peaking earlier at higher energies.

In all scenarios, the escape timescale t_{esc} and the effect of radiative cooling determine the decay times of the flares in different energy bands.

References

1. L. Maraschi, G. Ghisellini, A. Celotti, *Astrophys. J.* **397**, L5 (1992).
2. S. D. Bloom, A. P. Marscher, *Astrophys. J.* **461**, 657 (1996).
3. J. H. Matthews, A. R. Bell, K. M. Blundell, *New Astronomy Reviews* **89**, 101543 (2020).
4. A. Dmytriiev, H. Sol, A. Zech, *Monthly Notices of the Royal Astronomical Society* **505**, 2712–2730 (2021).
5. N. S. Kardashev, *Soviet Astronomy* **6** (1962).
6. A. Tramacere, E. Massaro, A. M. Taylor, *Astrophys. J.* **739**, 66 (2011).
7. J. S. Chang, G. Cooper, *J. Comput. Phys.* **6**, 1–16 (1970).
8. A. Tramacere, *JetSeT: Numerical modeling and SED fitting tool for relativistic jets*, Astrophysics Source Code Library, record ascl:2009.001, Sept. 2020.
9. A. B. Pushkarev, Y. Y. Kovalev, M. L. Lister, T. Savolainen, *Astron. Astrophys.* **507**, L33 (2009).
10. J. G. Kirk, F. M. Rieger, A. Mastichiadis, **333**, 452–458 (May 1998).